*Sensors & Transducers, Vol. 239, Issue 12, December 2019, pp. 34-40*

**Sensors & Transducers**

Published by IFSA Publishing, S. L., 2019
http://www.sensorsportal.com

# Non-invasive Optical Pressure Sensing using a Scalable Reflective Polydimethylsiloxane Membrane

**[1] Vitor A. V. ROSSI, [1, 2] and [*] Michael A. CARPENTER**

[1] SUNY Polytechnic Institute, College of Nanoscale Science and Engineering, 257 Fuller Road, Albany NY, 12203, USA

[2] SUNY Polytechnic Institute, College of Engineering, 100 Seymour Rd, Utica NY, 12203, USA

E-mail: mcarpenter@sunypoly.edu

*Received: 17 October 2019 /Accepted: 20 November 2019 /Published: 9 December 2019*

**Abstract:** Thin polydimethylsiloxane (PDMS) membranes have been employed as an optical reflectance-based pressure sensor. A unique PDMS membrane transfer method has been utilized using a polystyrene coated silicon wafer which allows for multiple uses and ease of scalable manufacturing of the device structures. The device is produced using the transfer method and common PDMS preparation and bonding techniques onto a glass substrate. Light intensity reflected off the membrane is recorded as pressure in the sensing environment changes, and a measurable reflectance intensity change is detected with a photodiode. Device testing in both dry and humid environments has shown a sensitivity of 0.6 millivolts per Torr, an 8.6 mTorr limit of detection and a 33 millisecond response time.

**Keywords:** Pressure, sensor, optical, polydimethylsiloxane, membrane

## 1. Introduction

Polydimethylsiloxane (PDMS) is a commonly and widely used polymer due to several advantages over other materials, including but not limited to high flexibility, cost effectiveness, biological and environmental compatibility (non-toxicity), chemical and mechanical robustness, hydrophobicity and ease of fabrication. These characteristics have allowed for the widespread use of PDMS in a broad range of scientific fields including microfluidics [1], soft lithography [2], sensor technology [3], protective coatings [4] and analytical chemistry [5].

Within the sensor technology field there has been increased usage of PDMS as the active component of devices, often replacing stiffer materials in order to take advantage of its flexibility. Piezoresistive sensors as an example measure a change in resistance of a deformable membrane given a pressure differential [6, 7]. PDMS has been used in this context as the diaphragm material resulting in highly sensitive devices [8–13], with limits of detection as low as 4.5 mTorr [12]. These types of devices require electronic components in order to operate, increasing the complexity required for packaging and integration. The intrusion of these components into the sensing environment can also cause issues by introducing contamination and leakage, which are detrimental in many fields.

For applications where electrical circuitry is unwanted, optical sensing provides a reliable alternative with different sensors and methods available. Devices using extrinsic Fabry-Perot interferometry are frequently reported [14–20], using a diaphragm attached at the end of an optical fiber. Measurable shifts in the reflectivity spectrum of the interferometer occur as deflection of the diaphragm arises due to pressure changes. Zhao et al. [20] took

advantage of the flexible nature of PDMS by building their devices with a polymeric membrane, reaching high sensitivities in the μTorr range. Improvement of this technology will clearly have broad applications; however, interferometers require precise optical alignment and complex integration schemes.

Pressure sensors which monitor the deformation of elastomer membranes for pressure sensing have been reported in the modern literature and a subset are discussed in the context of the present work [20–24]. This type of approach has been modeled in the literature for diaphragm based pressure sensors [25] as well as PDMS membranes [26]. Orth et al. [21] assembled 2D arrays of elastomer membranes enabling sensing of pressure fields in microfluidic devices, with sensitivity in the Torr range. Tsai & Kaneko [23] reported a pressure sensor based on PDMS deformation, which induced a change in color intensity of a colored fluid within a sensing chamber and focused on pressure sensing in the kilotorr range, with pressure waves of up to 16 Hz being detected. Chaudhury et al. [24] demonstrated a pressure sensor based on a PDMS membrane. Their device operated by pressurizing an internal sealed cavity causing a deflection in the membrane. The reflected light was collected with a CCD detector and the data was processed with a MATLAB image contrast algorithm in order to extract the pressure. The achieved resolution of 375 mTorr is not as remarkable as other sensors, but the ease of fabrication is desirable in order to scale production to real world applications. Given this body of work it is clear that ease of fabrication of PDMS membrane devices with enhanced sensing properties remains an active field of study within pressure sensor technology.

In the present work an optical PDMS-based pressure sensor with millitorr resolution was fabricated via scalable processing schemes. A previously developed methodology for rapid PDMS membrane fabrication was adopted [27], allowing reliable and reproducible sensor fabrication.. The devices performed well in both dry and humid environments reaching a lower limit of detection of 8.6 mTorr, enabling broad applications such as live monitoring of catalytic reactions [13] as well as pressure monitoring of drug delivery systems for glaucoma research [28, 29].

## 2. Experimental Methods

A critical aspect with regards to the sensor design and fabrication is the repeatable fabrication schemes that have been utilized for the reliable transfer of PDMS membranes. For the current work a polystyrene coated wafer has been adopted to serve as the membrane transfer substrate [27] and is described as follows. This approach was chosen based on literature of PDMS membranes produced on a polystyrene petri dish [30]. For thin PDMS membranes in the micron range, the non-uniformity of petri dish creates uneven films, so the choice of a uniform transfer substrate is highly desirable.

In order to circumvent the problems associated with the polystyrene petri dish, polystyrene pellets were dissolved in anhydrous toluene 99.8 % (Sigma Aldrich) resulting in a 2 % solution by weight. The solution was heated to 60 °C for 2 hours with continuous mixing in order to ensure full dissolution of the polymer. Silicon wafers were cleaned with piranha solution (3:1 $H_2SO_4$:$H_2O_2$) for 10 minutes, rinsed with DI water, dried with a nitrogen gun and were then used as the substrate. The wafers were placed on the spin coater and DI water was poured onto the surface until fully covered. They were then spun at 3000 RPM for 1 minute with a 3 second ramp up step. This step was employed in order to remove particles from the surface and dry the wafer. Once the first spin process ended, the polystyrene-toluene solution was immediately poured onto the Si wafer through a 0.22 μm pore size syringe filter fully covering the surface and spun using the same parameters. After spin coating was completed, the wafers were placed in a conventional oven at 60 °C overnight to ensure complete evaporation of the solvent, resulting in a thin uniform polystyrene layer over the entire surface of the wafer. This wafer serves as the membrane transfer substrate.

Polydimethylsiloxane (PDMS) used in the fabrication of the sensors is commercially available as Sylgard 184 silicone elastomer kit (Dow Corning Corporation). A base-curing agent (10:1 weight ratio) was mixed in a glass petri-dish, stirred with a spatula for 3-5 minutes and degassed with a roughing vacuum for 5-10 minutes until all bubbles disappeared. The sensors were produced from two components which were fabricated separately. For the first component (PDMS base) a glass slide cleaved into a square (2.5 by 2.5 cm) was used as the substrate. The substrate was cleaned using a conventional solvent rinse method including an acetone and an ethanol step. The substrate was thoroughly dried with a pressurized air gun and PDMS was poured over the entire surface. A second glass slide cleaned with the same method was lowered onto the PDMS, raised above the squared glass substrate by 1 mm. This flattens the PDMS creating a uniform film of 1 mm in thickness. The second component (PDMS membrane) was fabricated using the polystyrene coated wafer as the substrate. The wafer was placed on the spin coater and cleaned with DI water as previously described. PDMS was poured over the wafer covering most of the surface and spun at 1000 RPM for 1 minute with 10 seconds of ramp up time. For both base and membrane components, the PDMS was fully cured overnight in a conventional oven at 60°C. A profilometer was used to record the PDMS membrane thickness of 70 μm, which agreed with the estimated value for the spin coating parameters listed above.

To create the sensors, a circular cavity was stamped out of the center of the PDMS base and removed. Both membrane and base were simultaneously treated with $O_2$ plasma at

approximately 30 Watts and 200 mTorr operating pressure for 30 seconds. After venting the process chamber, the base was bonded onto the membrane wafer by bringing the two surfaces into contact. The bonded device was lifted off the wafer and excess membrane was removed. The polystyrene coated wafer serving as the transfer substrate for the PDMS membrane was able to be used repeatedly for multiple membrane samples.

Sensing was conducted in a system schematically depicted in Fig. 1. Fig. 1a and b show a side view of the assembled setup and an extruded view of the components respectively. An Ocean Optics lab-grade reflection probe was used to direct light onto the sample and to collect the reflected light, seen in Fig. 1b (1). The source light is transported via six individual fibers surrounding a seventh fiber which collects the reflected light. Each of these fibers is 400 µm in diameter, and the probe has an acceptance angle of 24.8° in air. The sensor depicted in Fig. 1b (3) was placed inside of the chamber Fig. 1b (4) and a removable glass window Fig. 1b (2) was used to seal the chamber. Light was transmitted through the glass window onto the device. Gas flow was controlled with an Environics Series 4000 gas mixing system, and the gas outlet was directed towards a two valve setup (Fig. 1c): a needle valve and an electronic solenoid valve. When the solenoid valve was open, the chamber pressure was held at atmospheric pressure. When the solenoid was closed, the gas flow was restricted through the needle valve causing the system pressure to increase to a predefined setpoint. Multiple pressure setpoints were controlled by increasing the gas flow rate, which in turn increased the chamber pressure when the solenoid was closed but had negligible effects when it was open. An MKS 910 DualTrans transducer was used to independently record the system pressure during the experiments.

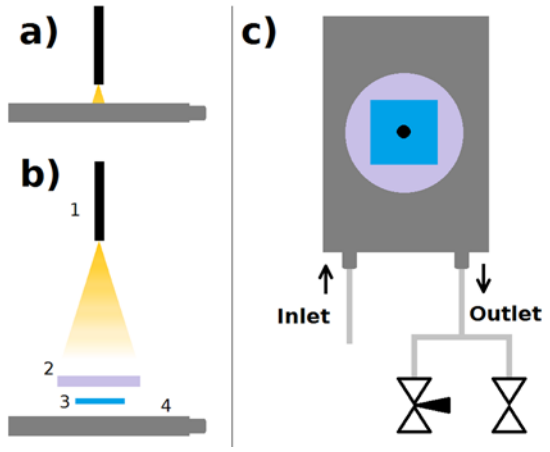


**Fig. 1.** Schematic of the pressure sensing bench: (a) Assembled side view; (b) Extruded side view where 1 is the optical fiber, 2 is the glass window, 3 is the sensor and 4 is the sensing chamber, and (c) Top view.

Sensing experiments were conducted while recording the reflected light intensity from the PDMS membrane. System pressures were varied between atmospheric to pressure setpoints of 0.5, 1, 1.5, 2, 2.5, 3, 4 and 5 Torr (above atmospheric). An Ocean Optics LS-1 white light source was used in the experiments and the reflected light was collected via the reflection probe and directed through a convergence lens onto a Melles Griot photodiode. The voltage generated by the photodiode was measured with an Agilent 34970A data acquisition unit. Custom Python scripts using the open source RPi.GPIO library were developed to control data collection and solenoid operation simultaneously via TTL signal communication through the Raspberry Pi GPIO interface.

## 3. Results & Discussion

The PDMS membrane in the sensor behaves as a parabolic mirror, which is the known shape thin membranes adopt under uniform load [31]. This deformation is a known phenomenon: it has been modeled for pressure sensor applications [25]; and for PDMS membranes in particular [26]. The intensity of light reflected off a curved membrane is characteristic of the unique deformation for a given pressure differential. In Fig. 2, a schematic of the convergence of reflected rays is presented. This was simulated in Python by calculating the angle between the incident rays and the membrane. The equation used to model thin curved membranes given a pressure differential has been previously reported in literature [31].

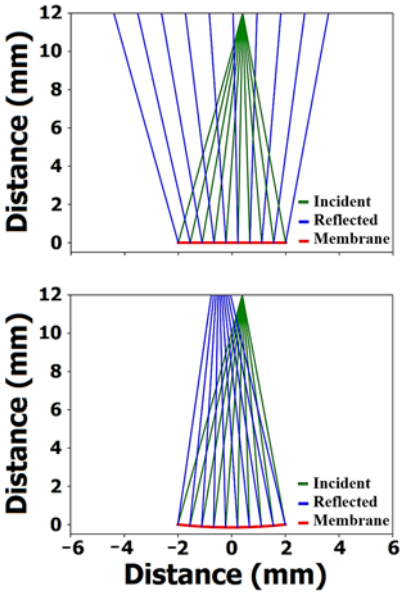


**Fig. 2.** Membrane deformation and ray tracing schematic of PDMS membrane under (a) atmospheric pressure $P_1$ and (b) $P_2 > P_1$.

From classical optics, the angle of the reflected rays with the normal equals that of the incident rays. With the system initially at atmospheric pressure (Fig. 2a) the membrane is expected to be nearly flat,

causing the reflected rays to diverge and the collected intensity to be less than the source intensity. When pressure in the surrounding environment is increased above atmospheric, the pressure differential between the sealed device cavity and the surroundings induces a deformation in the PDMS membrane shown schematically in Fig. 2b. This deformation causes the reflected rays to converge closer to the membrane with increasing pressure differential, which in turn generates the increase in reflected intensity. This behavior is expected for small membrane deformations only (low pressures). For larger deformations (high pressures) where the focal distance of the mirror is shorter than the probe distance, rays will diverge past the focal point and collected intensity would subsequently decrease with increasing deformation.

Fig. 3a shows the sensing trace of a pressure sensing experiment. Five 5-seconds on/off pressure cycles were conducted successively for each pressure set point (0.5, 1, 1.5, 2, 2.5, 3, 4 and 5 Torr) in a dry nitrogen environment. The baseline between cycles was collected at atmospheric pressure. The signal change of each cycle is well defined above the noise, even for the lowest pressure of 0.5 Torr. This discernible trend implies sub-Torr pressure resolution for the devices. To confirm this, a calibration curve shown in Fig. 3b was created by averaging 30 data points within each cycle and subtracting the averaged signal between pressure on and off. The five separate signal changes for each pressure setpoint were then averaged to yield the calibration points, with a final propagated error on the order of ±2 microvolts for each pressure (not visible on graphs). Based on the mean value and the estimated error, the signal to noise ratio was calculated to be 48 dB. From the linear calibration curve, the sensor sensitivity is equal to 0.41 millivolts per Torr, and the theoretical lower limit of detection (LOD) [32] is equal to 8.6 mTorr, calculated as three times the standard deviation of the measurements divided by the slope of the calibration curve. The linearity of the response is in agreement with literature [26] which showed a linear behavior for small PDMS membrane deformations.

The sensor response loses its linearity for pressures above 5 Torr. Initially, larger signal changes are noticed for fixed ΔP increases. At approximately 15 Torr the signal change reaches a maximum and begins to drop from there onwards with increasing pressure. This feature happens when the focal point of the curved membrane drops below the fiber probe distance, and reflected rays diverge instead of converging towards the collection probe. Fig. 4 shows one cycle of pressure change from atmospheric to 25 Torr. When the system pressurizes, signal increases and then decrease as the membrane sweeps through its pressure dependent deformations. When pressure is released, the opposite is noticed. It takes longer for the system to pressurize than to depressurize, which is the pressurization trend is more defined in this figure. This is discussed in more detail later.

Due to potential applications in biological and humid environments, the pressure test was also conducted in a high humidity nitrogen stream to ensure the device operation and sensitivity. The nitrogen flow was directed through a water reservoir in order to acquire water vapor content, and the test was conducted as described previously. Since the nitrogen flow was fully directed through the reservoir, nearly 100 % relative humidity was achieved. The system was allowed to stabilize overnight in humid nitrogen prior to testing. Fig. 5 shows the sensing trace and calibration curve for the same pressure setpoints as in the dry nitrogen experiment. Table 1 lists the averaged signal change between the five repeats for each set point.

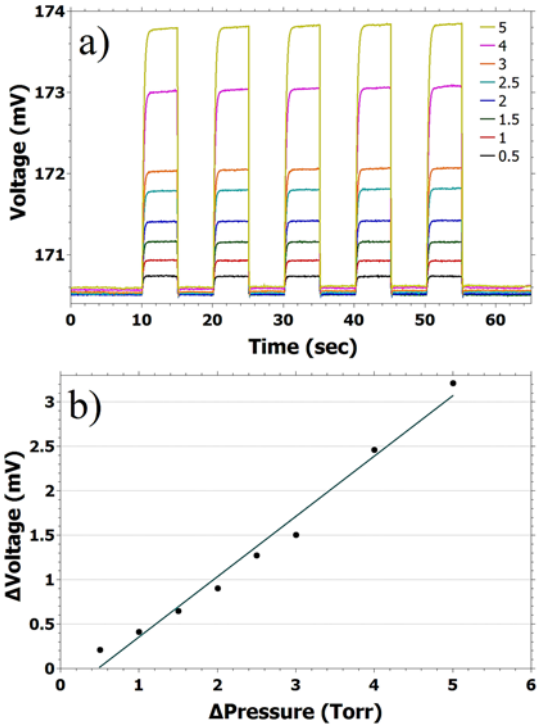


**Fig. 3.** (a) Sensing trace of a pressure sensing experiment in dry nitrogen with pressure set points of 0.5, 1, 1.5, 2, 2.5, 3, 4 and 5 Torr; (b) Calibration curve of the averaged signal change for each pressure set point.

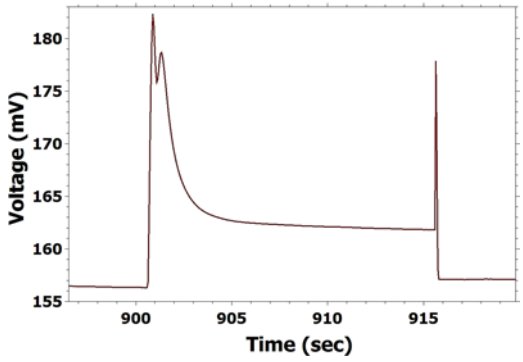


**Fig. 4.** Single repeat of pressure sensing at 25 Torr above atmospheric pressure.

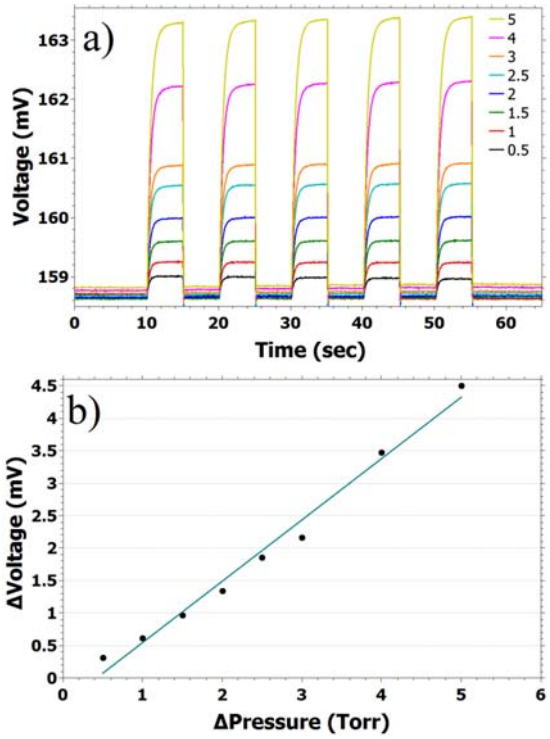


**Fig. 5.** (a) Sensing trace of a pressure sensing experiment in humidified nitrogen with pressure set points of 0.5, 1, 1.5, 2, 2.5, 3, 4 and 5 Torr; (b) Calibration curve of the averaged signal change for each pressure set point.

The sensor response in humid nitrogen is similar to the response in dry nitrogen, with a slight increase in sensitivity from 0.41 to 0.61 millivolts per Torr and propagated error on the order of ±2.8 microvolts. At elevated humidity levels, PDMS has been shown to aggregate water into the material [33], which leads to the decrease in the elastic modulus in polymers [34], [35] and thus the increase in sensitivity is consistent. In this experiment, signal to noise was estimated at 46 dB and the limit of detection was calculated to be 8.9 mTorr, which are nearly identical to that of the dry nitrogen experiment. It is important to note that the increase in signal for the humidified nitrogen test is reproducible, and the sample signal decreases again when tested in dry nitrogen.

**Table 1.** Averaged signal change for pressure sensing experiments in dry and humid nitrogen gas.

| ΔP (Torr) | Dry $N_2$ (mV) | $N_2 + H_2O$ (mV) |
|---|---|---|
| 0.5 | 0.21 | 0.31 |
| 1.0 | 0.41 | 0.61 |
| 1.5 | 0.65 | 0.97 |
| 2.0 | 0.91 | 1.34 |
| 2.5 | 1.27 | 1.86 |
| 3.0 | 1.51 | 2.16 |
| 4.0 | 2.47 | 3.47 |
| 5.0 | 3.21 | 4.50 |

It is difficult to determine the response time of the sensor given limitations with the current instruments; however, a response time discussion is warranted given its importance in typical applications. When the present system is pressurized by closing the electronic solenoid, the stored potential on the valve's coil is dissipated through a flyback diode. This means the system does not instantly reach the desired pressure setpoint. Additionally, given the low gas flow rates used for these setpoints (between 45 to 185 SCCM), a certain amount of time is required for the desired pressures to build up within the system. This is noticeable in the slow signal rise when the system is pressurized (Fig. 6a). On the other hand, when depressurizing the system, the electric potential is applied instantly to the solenoid and the pressure is released immediately (Fig. 6b). The first data point recorded in the present experiments is 33 milliseconds after the valve actuated and shows in all cases that the signal returned to the baseline, implying the response time was less than that of the data collection interval.

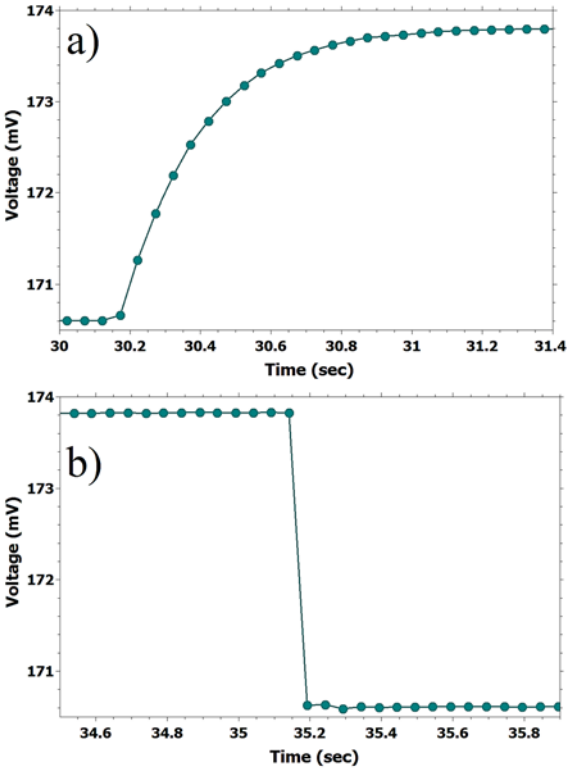


**Fig. 6.** (a) Signal rise during chamber pressurization; (b) Signal drop when system is brought to atmospheric pressure.

Another indication of the sensor's fast response was noticed while performing the humidity experiments. If the water level in the reservoir was filled too high, the nitrogen was forced to bubble through the water. When the bubbles burst on the reservoir's outlet, noise spikes were seen in the data. This effect is depicted in Fig. 7 where (a) shows five repeats for the 1 Torr pressure cycle and (b) shows a

closeup of the third repeat. The noise seen in the data was due to system pressure fluctuations caused by the bursting of $N_2$ bubbles. The periodicity of the noise increased with higher pressures, since larger gas flows were used to control these setpoints. The gas flow was directly related to the bubble bursting frequency.

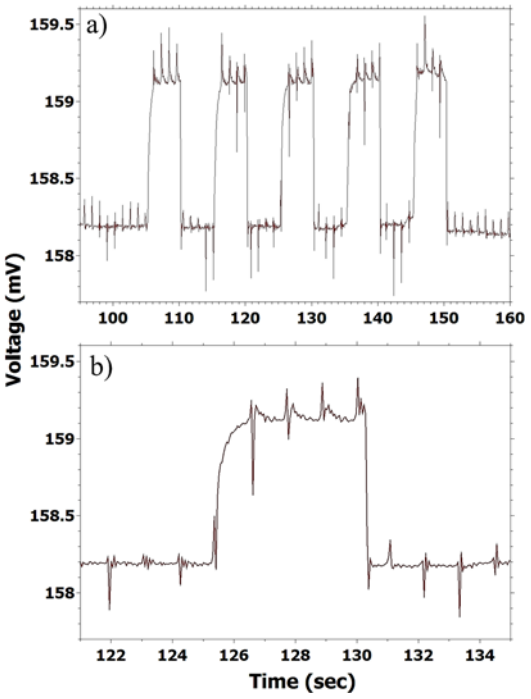


**Fig. 7.** (a) Five repeats of the 1 Torr cycle within a pressure sensing experiment; (b) Close up of the third repeat within the 1 Torr cycle. High noise is noticed in the data, attributed to the bursting of nitrogen bubbles within the system.

These results are encouraging for several reasons. The sensitivity achieved by our sensor is comparable with electronic devices [9] and although there are devices with higher sensitivity [12], the limit of detection observed in the present study is comparable. Furthermore, optical reflection based sensors from previously published membrane studies have not been able to achieve such sensitivities [14]–[19]. Our device is sealed inside of the sensing chamber and light generation and collection is non-invasive, realized completely from the outside. This eliminates the need of electrical wiring, elaborate light sources and fiber probe insertion into the sensing environment, which in turn eliminates contamination and potential leaks.

Possible applications of a pressure sensor with these attributes include real time monitoring of catalytic reactions [13] as well as glaucoma research, where changes in the internal pressure of a testing system relates to the treatment's efficacy [28], [29]. Furthermore, there is large room for improvement of this PDMS sensor considering this is a first-generation device. Future work will focus on improving sensitivity as well as measuring and fine-tuning response time limiting hardware and software. Optimization of membrane size and thickness will be explored, and the addition of 3D structures onto the membrane in order to measure wavelength dependency of the reflected light.

## 4. Conclusion

In this manuscript we proposed a new method for pressure sensing with sub-Torr sensitivity. We described the device production techniques which involve conventional PDMS preparation and bonding, with a unique reusable polystyrene coated wafer for PDMS membrane transfer. The PDMS membrane devices were tested in a sensing chamber with pressure setpoint control in order to generate a sensing trace. Calibration curves were constructed from the sensing data and a linear trend was discerned. Further data analyses revealed the sensor sensitivity of 0.41 and 0.61 millivolts per Torr and limit of detection of 8.6 and 8.9 mTorr for tests in dry and humidified nitrogen respectively.

## References

[1]. S. K. Sia and G. M. Whitesides, Microfluidic devices fabricated in poly(dimethylsiloxane) for biological studies, *Electrophoresis*, Vol. 24, No. 21, 2003, pp. 3563–3576.

[2]. K. Y. Kim, Pilnam, Kwon, Keon Woo, Park, Min Cheol, Lee, Sung Hoon, Kim, Sun Min, Suh, Soft Lithography for Microfluidics: a Review, *The Korean BioChip Society*, 2008.

[3]. S. Cichosz, A. Masek, and M. Zaborski, Polymer-based sensors: A review, *Polymer Testing*, Vol. 67, January 2018, pp. 342–348.

[4]. U. Eduok, O. Faye, and J. Szpunar, Recent developments and applications of protective silicone coatings: A review of PDMS functional materials, *Progress in Organic Coatings*, Vol. 111, May 2017, pp. 124–163.

[5]. S. Seethapathy and T. Górecki, Applications of polydimethylsiloxane in analytical chemistry: A review, *Analytica Chimica Acta*, Vol. 750, 2012, pp. 48–62.

[6]. C. Pramanik, H. Saha, and U. Gangopadhyay, Design optimization of a high performance silicon MEMS piezoresistive pressure sensor for biomedical applications, *Journal of Micromechanics and Microengineering*, Vol. 16, No. 10, 2006, pp. 2060–2066.

[7]. Y. Shu *et al.*, Surface-modified piezoresistive nanocomposite flexible pressure sensors with high sensitivity and wide linearity, *Nanoscale*, Vol. 7, No. 18, 2015, pp. 8636–8644.

[8]. D. W. Lee and Y. S. Choi, A novel pressure sensor with a PDMS diaphragm, *Microelectronic Engineering*, Vol. 85, No. 5–6, 2008, pp. 1054–1058.

[9]. L. Wang *et al.*, Polydimethylsiloxane-integratable micropressure sensor for microfluidic chips, *Biomicrofluidics*, Vol. 3, No. 3, 2009, pp. 1–8.

[10]. X. Liu, Y. Zhu, M. W. Nomani, X. Wen, T. Y. Hsia, and G. Koley, A highly sensitive pressure sensor using a Au-patterned polydimethylsiloxane membrane for

biosensing applications, *Journal of Micromechanics and Microengineering*, Vol. 23, No. 2, 2013, p. 025022.
[11]. L. Zhang, G. Hou, Z. Wu, and V. Shanov, Recent Advances in Graphene-Based Pressure Sensors, *Nano LIFE*, Vol. 06, No. 03n04, 2016, p. 1642005.
[12]. M. Jian *et al.*, Flexible and Highly Sensitive Pressure Sensors Based on Bionic Hierarchical Structures, *Advanced Functional Materials*, Vol. 27, No. 9, 2017.
[13]. A. Zizzari *et al.*, Highly Sensitive Membrane-Based Pressure Sensors (MePS) for Real-Time Monitoring of Catalytic Reactions, *Analytical Chemistry*, Vol. 90, No. 12, 2018, pp. 7659–7665.
[14]. T. W. Kao and H. F. Taylor, High-sensitivity intrinsic fiber-optic Fabry–Perot pressure sensor, *Optics Letters*, Vol. 21, No. 8, Apr. 1996, p. 615.
[15]. S. H. Aref, H. Latifi, M. I. Zibaii, and M. Afshari, Fiber optic Fabry-Perot pressure sensor with low sensitivity to temperature changes for downhole application, *Optics Communications*, Vol. 269, No. 2, 2007, pp. 322–330.
[16]. Q. Yu and X. Zhou, Pressure sensor based on the fiber-optic extrinsic fabry-perot interferometer, *Photonic Sensors*, Vol. 1, No. 1, 2011, pp. 72–83.
[17]. F. Xu *et al.*, High-sensitivity Fabry–Perot interferometric pressure sensor based on a nanothick silver diaphragm, *Optics Letters*, Vol. 37, No. 2, 2012, p. 133.
[18]. S. Silva, L. Coelho, and O. Frazão, An all-fiber Fabry-Pérot interferometer for pressure sensing in different gaseous environments, *Measurement: Journal of the International Measurement Confederation*, Vol. 47, No. 1, 2014, pp. 418–421.
[19]. Y. Ge, K. Cai, T. Wang, and J. Zhang, MEMS pressure sensor based on optical Fabry–Perot interference, *Optik*, Vol. 165, 2018, pp. 35–40.
[20]. Y. Zhao, M. Qing Chen, F. Xia, and R. Qing Lv, Small in-fiber Fabry-Perot low-frequency acoustic pressure sensor with PDMS diaphragm embedded in hollow-core fiber, *Sensors and Actuators, A: Physical*, Vol. 270, 2018, pp. 162–169.
[21]. A. Orth, E. Schonbrun, and K. B. Crozier, Multiplexed pressure sensing with elastomer membranes, *Lab on a Chip*, Vol. 11, No. 22, 2011, pp. 3810–3815.
[22]. W. Song and D. Psaltis, Optofluidic pressure sensor based on interferometric imaging, *Optics Letters*, Vol. 35, No. 21, 2010, p. 3604.
[23]. C. H. D. Tsai and M. Kaneko, On-chip pressure sensor using single-layer concentric chambers, *Biomicrofluidics*, Vol. 10, 2016, No. 2.
[24]. A. R. Chaudhury, A. K. Pantazis, and N. Chronis, An image contrast-based pressure sensor, *Sensors and Actuators, A: Physical*, Vol. 245, 2016, pp. 63–67.
[25]. A. Nallathambi and T. Shanmuganantham, Design of Diaphragm Based MEMS Pressure Sensor with Sensitivity Analysis for Environmental Applications, *Sensors & Transducers*, Vol. 188, No. 5, 2015, pp. 48–54.
[26]. B. Houaria and B. Chellali, Study of the mechanical behavior of a hyperelastic membrane, *Sensors & Transducers*, Vol. 168, No. 4, April 2014, pp. 108–112.
[27]. V. A. V Rossi and M. A. Carpenter, Reusable Polystyrene Wafer Coating as an Antiadhesive Layer for PDMS Thin Film Production, *Submitted to Materials Letters*, May 2019.
[28]. D. A. Ryskamp *et al.*, TRPV4 regulates calcium homeostasis, cytoskeletal remodeling, conventional outflow and intraocular pressure in the mammalian eye, *Scientific Reports*, Vol. 6, No. July, 2016, pp. 1–15.
[29]. K. Y. Torrejon *et al.*, Bioengineered glaucomatous 3D human trabecular meshwork as an in vitro disease model, *Biotechnology and Bioengineering*, Vol. 113, No. 6, 2016, pp. 1357–1368.
[30]. S.-K. Chae, J.-H. Ryoo, and S.-H. Lee, Thin and large free-standing PDMS membrane by using polystyrene Petri dish, *BioChip Journal*, Vol. 6, No. 2, Jun. 2012, pp. 184–190.
[31]. W. K. Schomburg, Introduction to Microsystem Design, 2nd ed., *Springer Berlin Heidelberg*, Berlin, Heidelberg, 2015.
[32]. A. Shrivastava and V. Gupta, Methods for the determination of limit of detection and limit of quantitation of the analytical methods, *Chronicles of Young Scientists*, Vol. 2, No. 1, 2011, p. 21.
[33]. S. J. Harley, E. A. Glascoe, and R. S. Maxwell, Thermodynamic study on dynamic water vapor sorption in sylgard-184, *Journal of Physical Chemistry B*, Vol. 116, No. 48, 2012, pp. 14183–14190.
[34]. A. J. Nolte, N. D. Treat, R. E. Cohen, and M. F. Rubner, Effect of Relative Humidity on the Young's Modulus of Polyelectrolyte Multilayer Films and Related Nonionic Polymers, *Macromolecules*, Vol. 41, No. 15, Aug. 2008, pp. 5793–5798.
[35]. L. Silva, S. Tognana, and W. Salgueiro, Study of the water absorption and its influence on the Young's modulus in a commercial polyamide, *Polymer Testing*, Vol. 32, No. 1, , 2013 pp. 158–164.

---

Published by International Frequency Sensor Association (IFSA) Publishing, S. L., 2019 (http://www.sensorsportal.com).